

**Dramatic enhancement of xuv laser output using a multimode gas-filled capillary waveguide**T. Mocek,<sup>1</sup> C. M. McKenna,<sup>2</sup> B. Cros,<sup>3</sup> S. Sebban,<sup>1</sup> D. J. Spence,<sup>2</sup> G. Maynard,<sup>3</sup> I. Bettaibi,<sup>1</sup> V. Vorontsov,<sup>1</sup> A. J. Gonsavles,<sup>2</sup> and S. M. Hooker<sup>2</sup><sup>1</sup>*Laboratoire d'Optique Appliquée (LOA), ENSTA-École Polytechnique, Chemin de la Hunière, 91761 Palaiseau, France*<sup>2</sup>*Department of Physics, Clarendon Laboratory, University of Oxford, Parks Road, Oxford OX1 3PU, United Kingdom*<sup>3</sup>*Laboratoire de Physique des Gaz et des Plasmas, Université Paris-Sud, Bâtiment 210, 91405 Orsay, France*

(Received 12 May 2004; published 7 January 2005)

We report a significant increase of the output of a 41.8-nm Xe<sup>8+</sup> laser achieved by means of multimode guiding of high-intensity femtosecond laser pulses in a gas-filled dielectric capillary tube. The optimized lasing signal from a 15-mm-long capillary was nearly an order of magnitude higher than that from a gas cell of the same length. Simulations of the propagation of the pump laser pulse in the capillary confirmed that this enhancement is due to reflections from the capillary wall, which increase the length of the Xe<sup>8+</sup> plasma column generated. The influence of gas pressure and focusing position on the lasing is also presented.

DOI: 10.1103/PhysRevA.71.013804

PACS number(s): 42.55.Vc, 52.38.Hb

In the past few years, there has been considerable interest in using small-scale, high-power, femtosecond lasers operating at high repetition rates to generate by optical field ionization (OFI) plasmas suitable as gain media for both recombination [1,2] and collisionally excited [3,4] lasers at extreme ultraviolet (xuv) wavelengths (<50 nm). For both classes of xuv lasers, the lifetime of the population inversion is very short and so the pumping must be in the form of a traveling wave. This can be achieved most easily by longitudinal pumping. The most serious issue of the longitudinal pumping geometry is the formation of a sufficient length of plasma for amplification of the x-ray photons to occur, since the Rayleigh length naturally limits the length of the amplifying medium to at best a few millimeters. The problem is further exacerbated by ionization-induced refraction of the pulse: the transverse electron density gradients created by the leading edge of the pulse lead to a rapid reduction in the peak intensity, thereby preventing formation of the required ion species. This issue is more crucial for collisional schemes since the formation of hot pumping electrons through the OFI process requires a longer wavelength and the absolute difference of the refractive index from unity of a low-density plasma increases approximately quadratically with wavelength. For example, the use of 820 nm radiation, as opposed to the 248 nm pump radiation often used for recombination schemes, increases this difference by approximately an order of magnitude.

In order to extend the gain length that can be achieved by longitudinal pumping, it is necessary to guide the pump pulse over many Rayleigh lengths. Several techniques for guiding laser pulses with peak intensities relevant to OFI laser schemes, 10<sup>16</sup>–10<sup>18</sup> W cm<sup>-2</sup>, have been investigated. These include guiding in hollow capillaries [5,6], relativistic channeling [7], and several types of plasma waveguide [8–10]. Recently, we have demonstrated lasing at 41.8 nm in Xe<sup>8+</sup> using a gas-filled capillary discharge waveguide [11]. When used purely as a waveguide, a current pulse of several hundred amperes and duration of approximately 1 μs is discharged through a capillary filled with hydrogen gas [12,13]. The capillary discharge forms a plasma channel [14] able to

guide high-intensity (>10<sup>17</sup> W cm<sup>-2</sup>) laser pulses over lengths of several centimeters [12,15]. In order to drive a short-wavelength laser within the plasma channel it is necessary to dope the hydrogen gas with the lasing gas. The 41.8-nm laser signal observed with a 30-mm-long capillary discharge waveguide filled with 120 mbar of a 1:3 Xe:H atom gas mixture was ~4 times larger than that achieved with a 4-mm-long gas cell containing 20 mbar of pure Xe [11]. The presence of hydrogen is expected [13] to decrease the small-signal gain coefficient of the Xe<sup>8+</sup> laser transition through partial preionization of the Xe by the discharge, reduction of the gain cross section resulting from the increased transition linewidth, and an increased rate of deexcitation of the laser levels. As a consequence, while the gain length of collisionally excited OFI lasers can be greatly increased by driving them within a gas-filled capillary discharge waveguide, the single-pass gain may not be increased by the same factor.

In this paper we report the demonstration of a significant increase of the gain length of a collisionally excited OFI laser by using a capillary filled with pure lasing gas. No discharge is employed. Our data show that under optimum conditions the output of the Xe<sup>8+</sup> laser from a gas-filled capillary is nearly an order of magnitude stronger than that achieved with a gas cell. The experimental results are compared to simulations of the propagation of the pump laser pulse through the capillary, which indicate that this enhancement is due to reflection of the pump laser from the capillary walls. The resulting multimode guiding of high-intensity femtosecond laser pulses through the gas-filled capillary has made it possible to substantially increase the length and volume of the 8-times-ionized plasma column for xuv amplification.

The experiment was performed at LOA using a 10-Hz multiterawatt Ti:sapphire laser system [16] delivering 34-fs pulses (full width at half maximum) with an energy on target of up to 1 J. The circularly polarized laser beam was focused onto the capillary or gas cell entrance by a spherical mirror of focal length 2 m used in an off-axis configuration. The aberrations arising from the use of a spherical mirror were

corrected with a bimorph deformable mirror [17]. The measured transverse intensity distribution was close to a Gaussian distribution in the focal plane, with a central spot corresponding to a waist  $W_0$  (the radius at which the intensity falls to  $1/e^2$  of the axial intensity) of  $28 \pm 2 \mu\text{m}$  containing  $\sim 40\%$  of the energy in the plane. The laser beam was measured to be 1.6 times diffraction limited, the measured Rayleigh length was 3 mm, and the resulting maximum intensity on target was  $(1 \pm 0.2) \times 10^{18} \text{ W cm}^{-2}$  in vacuum. All results presented in the present paper were obtained with this peak input laser intensity. The 34-fs driving laser pulse was preceded by a 1-ns-long amplified spontaneous emission (ASE) pedestal with a measured energy of approximately  $2 \times 10^{-8}$  of that of the main pulse. The intensity of the ASE pedestal was therefore about 12 orders of magnitude weaker in intensity than the main pulse, and hence ablation and ionization of the capillary wall by the pedestal can be ignored. The experimental setup was similar to that described in Ref. [11]. The infrared radiation leaving the capillary or cell was reduced in intensity by reflections from two optically flat wedges, rendered parallel by a lens, and imaged onto a 12-bit charge-coupled device (CCD) camera by another lens and a microscope objective. The beam transmitted by the second wedge was focused onto a pyroelectric energy meter to determine the energy transmitted by the capillary or cell. The energy of the laser pulses entering the capillary was measured using a calibrated photodiode, and the transmitted energy was determined by comparing the measured input and output energies with those recorded when the capillary was replaced by a large diameter evacuated pipe. The on-axis xuv radiation was recorded by moving the first wedge out of the beam path, thereby allowing the radiation to enter the transmission grating spectrometer. The spectrometer comprised a grazing-incidence gold-coated spherical mirror, transmission grating with 2000 lines/mm, and a back-illuminated xuv CCD camera. Stray light from the driving laser was blocked by two  $0.3\text{-}\mu\text{m}$ -thick aluminum filters.

The capillaries used were 15 mm long, with an internal diameter of  $300 \pm 10 \mu\text{m}$ . Since the channels were laser machined, the walls of the capillaries were not optically smooth, but contained nonuniformities with typical dimensions of 5  $\mu\text{m}$ . Xe gas was flowed into the capillary through channels approximately 500  $\mu\text{m}$  wide and 250  $\mu\text{m}$  deep located 1.5 mm from each end. By injecting the gas in this way, the pressure in the main body of the capillary between the gas slots was uniform.

In order to compare the output lasing signal from the capillary with that obtained in previous work [18], we also investigated lasing in Xe cells of 4, 10, and 15 mm lengths. The entrance and exit windows of the cells were made of thin glass plates through which pinholes ( $\sim 0.5$  mm in diameter) were drilled by the pump laser at the beginning of each experimental session. The xuv laser signals obtained from the waveguide and gas cells were optimized by varying the gas pressure and the position of the vacuum focus of the pump laser. Under optimum pumping conditions the  $41.8\text{-nm}$   $\text{Xe}^{8+} 5d-5p$  lasing transition completely dominated the on-axis spectrum for both the cell and capillary waveguide. Figure 1 compares optimized output signals from the cell at 17 Torr (squares) and the capillary at 17 (solid triangles) and 30

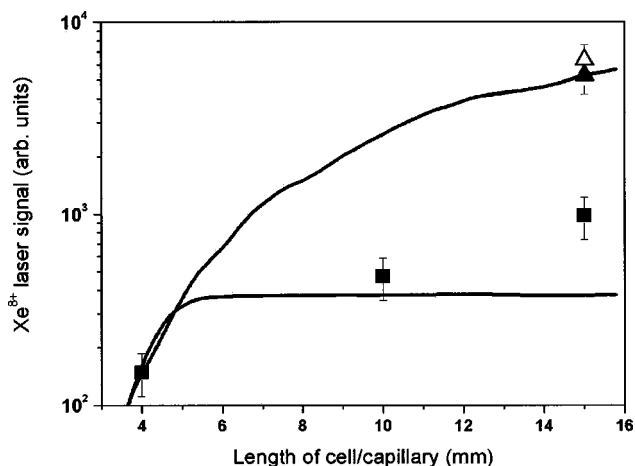


FIG. 1. Measured and simulated (solid lines)  $\text{Xe}^{8+}$  laser signal from the capillary at 17 (solid triangle) and 30 Torr (open triangle), respectively, and the cell at 17 Torr (squares) as a function of the cell or capillary length.

Torr (open triangles), respectively, as a function of target length. The position of the vacuum focus was 5 (6) mm inside the cell (capillary). The data in Fig. 1 were obtained with different filter sets which were cross calibrated using data obtained under nominally identical conditions. The solid curves present results of simulations which will be discussed later. The data clearly show that the capillary greatly increases the lasing signal compared to that achieved with a gas cell. The strongest signal was observed with the 15-mm-long capillary at 30 Torr, being approximately 7 times higher than the largest signal achieved with the cell of the same length and as much as 43 times higher than that with the 4-mm cell.

Figure 2 reports the measured pressure dependence of the  $\text{Xe}^{8+}$  laser signal for a 15-mm-long capillary (triangles) and a 15-mm-long cell (squares); the dashed and dotted lines are a guide to the eye. The position of the vacuum focus was at the center (entrance) of the cell (capillary). It is seen that in both cases the xuv laser signal exhibits a distinct optimum pres-

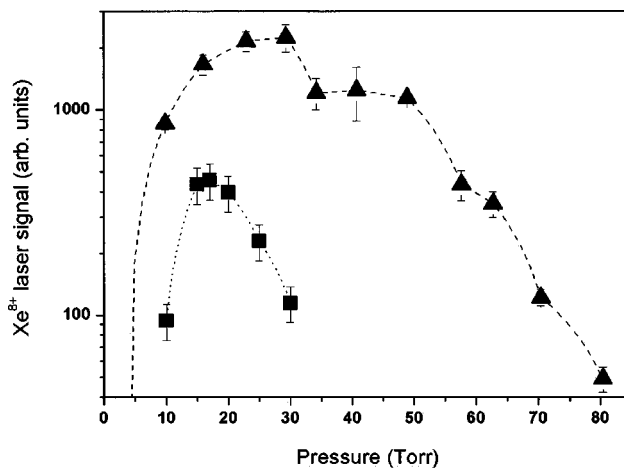


FIG. 2. Pressure dependence of the 41.8-nm lasing line for the 15-mm-long capillary (triangles) and the 15-mm-long cell (squares); the dashed and dotted lines are a guide to the eye.

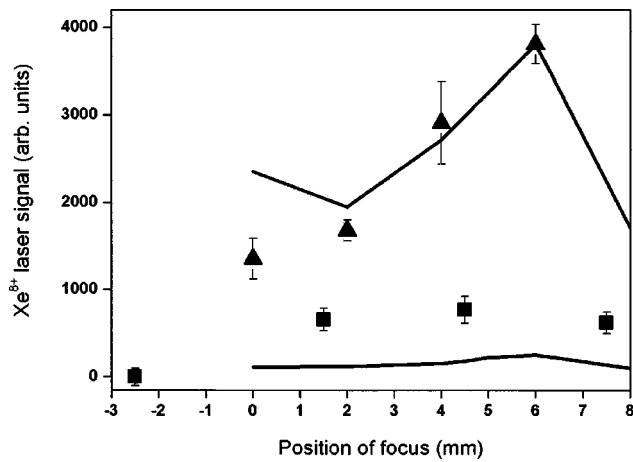


FIG. 3. Measured dependence of the lasing signal on the position of the vacuum focus of the pump laser for the capillary (triangles) at 30 Torr and the cell (squares) at 17 Torr compared with simulations (solid lines).

sure:  $30 \pm 5$  Torr for the capillary compared to  $17 \pm 2$  Torr for the cell. Apart from a significantly higher optimum pressure, the other main feature of the capillary lasing is that it occurred over a much broader range of pressures than for the gas cell: 10–70 Torr for the capillary compared to 10–30 Torr for the cells. There was no significant difference in the pressure dependence of the  $\text{Xe}^{8+}$  laser signal from the 4-, 10-, and 15-mm cells, the present results being consistent with earlier results for 4-mm-long cells [18].

The laser signal was also dependent on the position of the vacuum focus of the pump laser relative to the entrance of the target. Figure 3 shows the measured variation of the  $\text{Xe}^{8+}$  laser signal as a function of the position of the vacuum focus for a 15-mm-long capillary at 30 Torr (triangles) and a 15-mm-long cell at 17 Torr (squares). For the 15-mm-long cell the optimum position of the vacuum focus was found to be  $5 \pm 1$  mm inside the cell, though the dependence was weak (the signal for focal positions of 1.5 and 7.5 mm are  $\sim 85\%$  of the maximum signal at 5 mm). By contrast, in the case of the 15-mm-long capillary the signal was found to be quite sensitive to the focal position with a distinct optimum at 6 mm. Further, when the laser focus was set at 8 mm the capillary was destroyed in a relatively low number of pump laser shots. In the case of the 4-mm-long cell we did not find any clear optimum and the output signal was rather insensitive to the focusing position, in contrast to earlier work with a 1-m-focal-length optic [18]. This difference arises from the fact that use of a longer focal length optic extends the Rayleigh range, and hence the spot size and divergence of the beam at the entrance to the target are less sensitive to the position of the vacuum focus.

A numerical simulation code was used to model the propagation of high-intensity laser pulses through Xe gas undergoing optical field ionization, for both the capillary and cell targets. The code simulates the time-dependent propagation of the driving pulse in a three-dimensional (3D) cylindrically symmetric geometry and has been developed from the code described in Ref. [19]. The laser pulse is assumed initially to have Gaussian spatial and temporal profiles. The

paraxial wave equation is solved in cylindrical geometry to describe its propagation through the initially neutral gas, and the gas ionization is taken into account self-consistently. The pulse may be arbitrarily polarized and the effects of ionization-induced refraction as well as relativistic self-focusing are included. Hydrodynamic effects within the plasma are assumed to be insignificant on the femtosecond time scales of propagation and as such are not taken into account.

For the calculations presented here the circularly polarized pump laser pulse was assumed to have a Gaussian temporal profile with a full width at half maximum (FWHM) duration of 34 fs and a peak input intensity of  $1 \times 10^{18} \text{ W cm}^{-2}$ . The incoming laser field was taken as a sum of several (typically nine) Gaussian propagating modes as the best fit of the experimentally measured fluence profile in several planes before and after the best focal plane in vacuum. In the case of propagation inside the capillary, a boundary layer with a dielectric constant larger than 1 was introduced to simulate the capillary wall. Its value was adjusted so as to reproduce the measured value of the transmitted pump energy which is about 40% at a pressure of 25 Torr. By scaling these data we inferred an energy transmission of  $\sim 80\%$  at 17 Torr. A pressure of 17 Torr was selected for the simulations for both the capillary and gas cell since the small-signal gain coefficient and saturation intensity have been measured for this Xe pressure [18]. As seen in Fig. 2, for the capillary the  $\text{Xe}^{8+}$  laser output is relatively insensitive to the Xe pressure.

Figure 4(a) shows the calculated distribution of Xe ion stages following the passage of the pump laser pulse through a 15-mm-long cell under the conditions found experimentally to produce the largest  $\text{Xe}^{8+}$  laser signal—i.e., a pressure of 17 Torr and a focusing position of 6 mm inside the cell. It is seen that  $\text{Xe}^{9+}$  and higher ion stages are created in a small region around the axis for distances  $z$  of up to  $\sim 2$  mm from the entrance. The lasing ion stage  $\text{Xe}^{8+}$  is generated in an annular region up to  $z=8$  mm and outside the degree of ionization decreases. Simulations performed for focusing positions less than 6 mm exhibited similar distributions of Xe ion stages to the one in Fig. 4(a), but the length and volume of  $\text{Xe}^{8+}$  was progressively smaller, in agreement with the experimentally observed slow decrease of the output laser signal (Fig. 3). No further enlargement of the  $\text{Xe}^{8+}$  region was found for focusing positions beyond 6 mm.

Figure 4(b) shows the calculated distribution of Xe ion stages inside the capillary under the same conditions as in Fig. 4(a). It is seen that  $\text{Xe}^{8+}$  is produced along the whole length of the capillary in an annular region with higher ion stages being generated in an approximately cylindrical region of radius  $\sim 20 \mu\text{m}$  along most of the capillary axis. By comparing Figs. 4(a) and 4(b) it is clear that the volume of the  $\text{Xe}^{8+}$  region is increased substantially for the capillary. The size of the  $\text{Xe}^{8+}$  region was found to be much more sensitive to the focusing than in the case of the cell, in agreement with the measured data for the capillary presented in Fig. 3. For the focusing position of 6 mm inside the capillary the region of  $\text{Xe}^{8+}$  created was the largest, with much less  $\text{Xe}^{7+}$  than when focusing at the entrance.

To quantitatively evaluate the performance of the studied

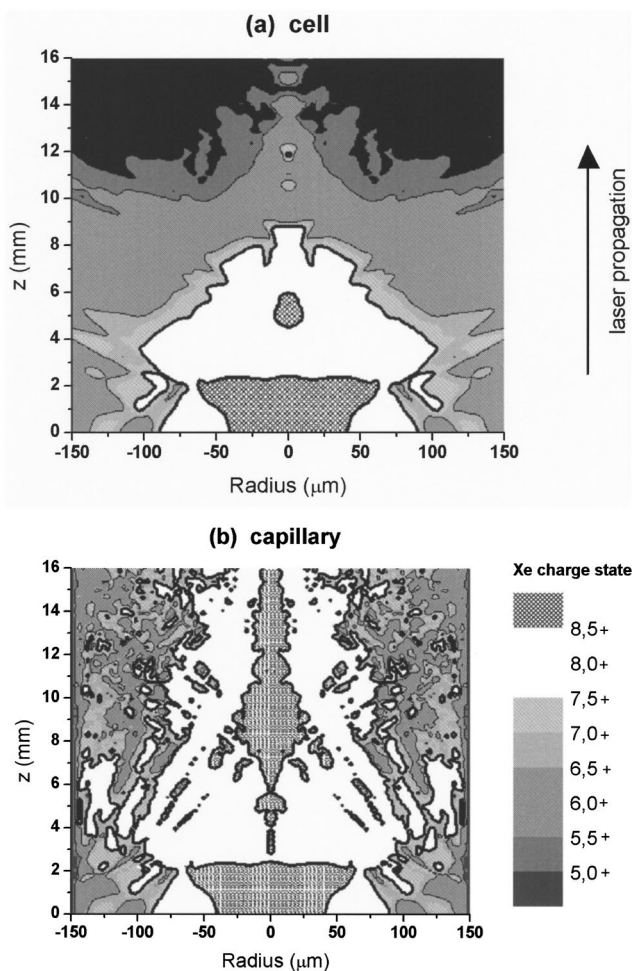


FIG. 4. Calculated distribution of Xe charge states following the passage of the pump laser pulse for a 15-mm-long (a) cell and (b) capillary. For both calculations the position of the vacuum focus was 6 mm inside the target and the pressure was 17 Torr.

xuv laser, we undertook simplified modeling of the radiation transfer in the active medium. The model treats amplification of axial emission in an active medium which accounts for the refraction of the xuv laser beam. It is assumed that both the small-signal gain ( $G_0$ ) and the emissivity ( $J_0$ ) are constant along the amplifier axis  $z$ . The output intensity  $I(z)$  can be expressed as [18]

$$\frac{\partial I}{\partial z} = gI + J_0, \quad (1)$$

where

$$g(z) = \frac{G_0}{1 + I(z)/I_{sat}} \quad (2)$$

is the large-gain coefficient and  $I_{sat}$  is the saturation intensity. The trajectory of an xuv beam in a medium with an electron density gradient  $\nabla n_e(\mathbf{r})$  is described by the ray equation

$$\frac{d}{ds} \left( n \frac{d\vec{r}}{ds} \right) = \vec{\nabla} n(\vec{r}), \quad (3)$$

where  $n$  is the plasma refraction index and  $ds = \sqrt{x^2 + y^2 + z^2}$ . Equation (3) is treated in the paraxial approximation which is justified by the very small radius of the lasing medium compared to its total length and the saturation length. The set of equations (1)–(3) is solved numerically to determine the output intensity  $I(z, r, \theta)$  using the plasma density profiles derived from the propagation code. The parameters  $G_0$ ,  $J_0$ , and  $I_{sat}$  entering Eqs. (1) and (2) should be considered to be averaged over all the dynamical phenomena. For the calculations presented here the values of  $G_0$  and  $J_0/I_{sat}$  were determined so that the solutions of Eqs. (1)–(3) reproduce closely the experimental gain curve in Ref. [18]. Within the fully dynamical model of [20], we have checked that for the few ps duration of the local gain [21], our simple model well reproduces the results of a one-dimensional dynamical model of the xuv amplification over distances larger than 1 mm using constant values for  $G_0$  and  $J_0/I_{sat}$ . In particular, for plasma lengths larger than 4 mm the influence of dynamical effects are greatly reduced because system is well inside the saturation regime as confirmed by both simulations and experimental results. It was found that the contribution of xuv propagation in the negative direction plays a negligible role, and so only the photons traveling in the positive direction are considered in Eqs. (1)–(3). Despite the relative simplicity of the model remarkably good agreement between the calculated and measured values of the Xe<sup>8+</sup> laser output signal was found.

In Fig. 1 results of simulations for the capillary and the cell are shown (solid lines), the normalization constant being the same for both simulations (that which gives the measured xuv laser signal from the capillary at 17 Torr). It is seen that the curve calculated for the cell agrees well with the experimental points for the 4- and 10-mm cells, and the two curves coincide for short lengths, as they should. The main discrepancy with the experimental results is that the simulated signal for the cell does not change after  $z=8$  mm since it is calculated that Xe<sup>8+</sup> is not generated for values of  $z$  greater than this, while the measured signal for the 15-mm cell is about 2 times larger than that for the 10-mm cell. This effect cannot be explained by the present modeling. Figure 3 compares the measured and calculated dependences of the xuv laser signal from the cell and capillary on the position of the vacuum focus of the pump laser. For both types of target the calculations show a distinct optimum for focal positions approximately 6 mm inside the target. Further, the much stronger influence of the focal position for the capillary is well reproduced by the modeling. The discrepancy between the simulated curve and experimental data in the case of the cell is mainly due to the difference already observed in Fig. 1 between 10 and 15 mm.

It should be emphasized that the guiding of the pump radiation observed in the present work is quite different from the monomode guiding observed previously for evacuated and gas-filled capillaries [6,22]. In order to achieve monomode guiding the spot size of the pump laser pulse at the capillary entrance must be carefully matched to the diameter

of the capillary. Abrams [23] has shown that optimum coupling into the lowest-order mode of the capillary occurs for a Gaussian beam when the input waist size is 0.6435 times the capillary radius. In the present work the laser spot radius at the capillary entrance was  $\sim 0.2$  times the capillary radius, so multimode guiding is expected to occur. As the wall of the capillary was not optically smooth, losses are expected to be higher than for a smooth inner surface. Furthermore, guiding is likely to be highly multimode when the gas ionization by the laser pulse results in a partially ionized medium and large transverse density gradients, as will have occurred in the present experiments. Nevertheless, the resultant guiding of pump pulses allows the length and volume of the  $\text{Xe}^{8+}$  gain region to be extended significantly, with a consequently large increase of the xuv laser output. The calculations presented here show that this enhancement was achieved by reflections of the pump laser radiation from the capillary wall and that this resulted in a substantial increase of the length and volume of the lasing ion stage and an increase in the xuv signal by more than one order of magnitude. In conjunction with evidence from previous experiments [18] and from agreement with the simulations, we deduce that the emission is well above the saturation value.

The gas-filled capillary also has several practical advantages over the cell. The capillary provides a differential pumping geometry in a straightforward way, and the gas pressure drops between the gas injection points and the ends of the capillary, rather than across an aperture, so for the same diameter hole the gas flow into the chamber is lower for the capillary than for a pinhole. The sapphire capillaries

employed in the present experiments were robust and had a long lifetime. For example, one capillary was used for over 1000 laser shots and only suffered damage when the laser was focused 8 mm inside the capillary. Capillary targets of this type are likely to be very useful in the search for lasing on other OFI laser transition and will complement other guiding techniques that can be employed to drive xuv lasers [11].

In summary, we have demonstrated significant improvement of the OFI  $\text{Xe}^{8+}$  laser performance by employing multimode guiding of femtosecond laser pulses with an intensity of  $\sim 10^{18}$  W cm $^{-2}$  through a gas-filled capillary. The optimized xuv laser signal from the capillary was nearly an order of magnitude stronger than that from a gas cell of the same length. Simulations of the propagation of the pump laser pulse through the capillary confirmed that this enhancement is due to reflections from the capillary wall, which resulted in a substantial increase of the length and volume of the  $\text{Xe}^{8+}$  plasma column, and so large improvement of the xuv beam quality can be expected. Direct measurement of the far-field pattern and related beam properties of the capillary-driven  $\text{Xe}^{8+}$  laser will be the subject of future investigations.

The authors acknowledge invaluable technical support from the laser staff at LOA. A.J.G. and C.M.M. are grateful to the EPSRC for support. T.M. is supported by the European Commission (Contract No. HPMF-CT-2002-01554) and S.M.H. by the Royal Society. This work was supported by the European Community, Access to Research Infrastructure action of the Improving Human Potential Programme, Contract No. HPRI-1999-CT-00086.

- 
- [1] Y. Nagata *et al.*, Phys. Rev. Lett. **71**, 3774 (1993).  
 [2] B. N. Chichkov *et al.*, Phys. Rev. A **52**, 1629 (1995).  
 [3] B. E. Lemoff *et al.*, Phys. Rev. Lett. **74**, 1574 (1995).  
 [4] S. Sebban *et al.*, Phys. Rev. Lett. **89**, 253901 (2002).  
 [5] S. Jackel *et al.*, Opt. Lett. **20**, 1086 (1995).  
 [6] F. Dorchies *et al.*, Phys. Rev. Lett. **82**, 4655 (1999).  
 [7] P. Monot *et al.*, Phys. Rev. Lett. **74**, 2953 (1995).  
 [8] C. G. Durfee and H. M. Milchberg, Phys. Rev. Lett. **71**, 2409 (1993).  
 [9] Y. Ehrlich *et al.*, Phys. Rev. Lett. **77**, 4186 (1996).  
 [10] T. Hosokai *et al.*, Opt. Lett. **25**, 10 (2000).  
 [11] A. Butler *et al.*, Phys. Rev. Lett. **91**, 205001 (2003).  
 [12] A. Butler *et al.*, Phys. Rev. Lett. **89**, 185003 (2002).  
 [13] D. J. Spence *et al.*, J. Opt. Soc. Am. B **20**, 138 (2003).  
 [14] N. A. Bobrova *et al.*, Phys. Rev. E **65**, 016407 (2002).  
 [15] D. J. Spence *et al.*, J. Phys. B **34**, 4103 (2001).  
 [16] M. Pittman *et al.*, Appl. Phys. B: Lasers Opt. **74**, 529 (2002).  
 [17] T. A. Planchon *et al.*, Opt. Commun. **216**, 25 (2003).  
 [18] S. Sebban *et al.*, J. Opt. Soc. Am. B **20**, 195 (2003).  
 [19] S. C. Rae, Opt. Commun. **97**, 25 (1993).  
 [20] F. Strati *et al.*, Phys. Rev. A **64**, 013807 (2001).  
 [21] T. Mocek *et al.*, Appl. Phys. B: Lasers Opt. **78**, 939 (2004).  
 [22] B. Cros *et al.*, IEEE Trans. Plasma Sci. **28**, 4 (2000).  
 [23] R. L. Abrams, IEEE J. Quantum Electron. **8**, 838 (1972).